

NAL PROPOSAL NO. 9B

Correspondent: M.L. Stevenson

University of California
Lawrence Berkeley Laboratory
Berkeley, California 94720
Telephone: FTS-18-415-843-6301
Commercial: 415-843-2740 Ext. 6301

PROPOSAL TO STUDY NEUTRINO INTERACTIONS IN THE
30 m³ NAL BUBBLE CHAMBER WITH EXTERNAL
MUON IDENTIFIER

R.J. Cence, F.A. Harris, M.W. Peters, V.Z. Peterson
V.J. Stenger, and D.E. Ycunt
University of Hawaii

M. Alston-Garnjost, S.I. Parker, F.T. Solmitz, and M.L. Stevenson
University of California
Lawrence Berkeley Laboratory

July 9, 1971

PROPOSAL TO STUDY NEUTRINO INTERACTIONS IN THE
30 m³ NAL BUBBLE CHAMBER WITH EXTERNAL
MUON IDENTIFIER

ABSTRACT

We propose: 1) to participate in the development of a muon identifier external to the NAL 30 m³ bubble chamber, 2) to use the external muon identifier with a narrow band beam and hydrogen filling to investigate, at energies above 20 GeV, neutrino total cross sections, deep-inelastic scattering, and possible W production, and 3) to use the external muon identifier with a broad-band beam and hydrogen filling to investigate individual neutrino reaction channels with good statistics over a broad range of energies. At this time, specifically, we request bubble chamber exposures yielding 5,000 neutrino events and 5,000 anti-neutrino events with the narrow-band beam and 50,000 events with the broad-band neutrino beam. Requests for exposure to deuterium and neon will be deferred until more is known about the bubble chamber operation.

I. INTRODUCTION

Our original proposal to study high energy (15-80 GeV) neutrino interactions in the 30 m³ NAL bubble chamber (NAL Proposal No. 9)¹ contains two unique features: 1) a proportional quantameter to detect photons from neutral pions produced in neutrino interactions and 2) an external muon identifier (EMI) to detect penetrating muons. The proportional quantameter would be installed immediately downstream of the hydrogen vessel between the vessel and the magnet coils, and a significant modification of the bubble chamber would be required. The EMI would consist of detector planes having spatial resolution, these planes interspersed with absorbing walls external to the bubble chamber. The EMI could be developed essentially independently of the bubble chamber.

Since our original proposal was submitted more than one year ago, two major developments have occurred. First, the quantameter has been deferred.² This implies that the fraction of the neutrino energy that goes into neutral pions, and thus into photons, will not be detected with good efficiency. We therefore propose to carry out those measurements requiring a knowledge of incident neutrino energy, such as total cross sections and deep inelastic scattering, using a narrow-band neutrino beam.*

The second major development has been the approval and partial funding by NAL of the external muon identifier. This decision reflects the broad support within the bubble chamber community for a muon identifier and is due also to the considerable progress made during the last year in designing and testing an EMI that promises to be both economical and highly efficient.³

The simultaneous use of the EMI and a narrow-band beam will permit a determination of both the incident neutrino energy and the momentum transfer to the final muon, as required in studying deep-inelastic scattering. Neither

* We shall attempt to develop techniques using the wide band data to obtain approximations to the neutrino energy.

the momentum transfer squared, Q^2 , nor the energy transfer, $\nu = E - E'$, can be determined without muon identification. In fact, it is in the region of Q^2 and ν where one is probing most deeply the structure of the target proton namely, large Q^2 and ν (with resulting large hadron multiplicities) that the identification becomes most difficult without an adequate EMI. The EMI will also be useful with a broad-band neutrino beam, and in this case, we propose to use the much higher broad-band flux to obtain good statistics on individual reaction channels, particularly those channels in which the final nucleon can be identified.

For the narrow-band experiment we request an exposure yielding 5000 events from π^+ neutrinos and 5000 events from π^- anti neutrinos. Pions and Kaons produced by 400-GeV protons will be selected at 100 ± 5 GeV/c to produce pion-neutrino at 43 ± 7 GeV and kaon-neutrinos at 96 ± 10 GeV.* Requests for an exposure to deuterium will be deferred until more is known about the bubble chamber operation. With 3×10^{13} incident protons per pulse on a one mean free path thick target, we estimate that for a neutrino cross section that continues to rise linearly with energy above 10 GeV, a run of 180,000 (260,000) pictures will yield 5,000 neutrino events (anti-neutrino events) in the 43-GeV bin and - 300 events in the 96-GeV bin.

For the broad-band experiment we request an exposure yielding 50,000 events. Of this number, more than 5,000 are expected to be above 30 GeV.⁴ For 10^{13} interacting protons per pulse at 400 GeV, approximately 50,000 pictures will be required.

* It is probable that we will run part of this exposure at lower energies. The results of the counter neutrino experiments will determine the optimum energies.

II. Physics Justification

The hybrid bubble chamber with its ability to look in detail at the structure of the final hadron state in inelastic neutrino scattering can resolve many of the questions that will be raised by the early neutrino counter experiments.

The conventions and definitions used in inelastic electron scattering and by Bjorken and Paschos⁵ are useful here. They are briefly:

Momentum transfer squared, Q^2 ,

$$Q^2 = 2M\nu + M^2 - W^2 ; \quad (1)$$

where M^2 and W^2 are the invariant mass squared of the initial and final hadron states respectively.

Energy transfer, ν ,

$$\nu = E - E' , \quad (2)$$

where, E and E' are the initial and final lepton laboratory energies respectively.

Lepton scattering angle, θ , (laboratory)

$$\sin^2 \frac{\theta}{2} = \frac{Q^2}{4EE'} \quad (3)$$

Hadron final state "scattering angle", θ_H (laboratory)

$$\sin^2 \theta_H = \left[\frac{E'}{E} \frac{\cos^2 \theta/2}{1 + (\nu^2/Q^2)} \right]^{1/2} \quad (4)$$

From these expressions the graphical display of Figure 1 can be constructed.

The straight lines radiating from the point $Q^2=0, \nu=20$ GeV are loci of equal muon scattering angles for 20 GeV neutrinos. The muon's laboratory energy can be easily found from $E' = 20 - \nu$. The solid parallel lines are loci of equal invariant hadron-mass W . The numbers, $\langle n_\pi \rangle$, are crude upper limits to the total pion multiplicity to be expected from hadron states of mass W . The dashed parabolic curves give values of δ_W^1 and can be used to derive crude upper limits to the "hadron jet" opening half-angle,

$\theta' \approx \gamma_w^{-1}$. Fig. 2 summarizes the appearance of typical events at the vertex of the interaction before the bubble chamber magnetic field sweeps them apart. The vector with the arrow is the muon momentum. The cones are for the hadron jets with half angle, γ_w^{-1} . The variables x and y are closely related to Q^2 and ν , respectively, and will be discussed in the following section. The manner in which the magnetic field sweeps these muons from their original direction is shown in Fig. 3. For emphasis we have indicated in each sub-sketch of Fig. 3 a number which is an upper limit of the expected pion multiplicity accompanying each of the muons. More will be said of their average behavior in section IV. The solid line trajectories correspond to muons produced to the left and right in the equatorial plane. The dashed trajectories are those muons produced with maximum dip angle.

A. Differential and total cross section.

The differential cross section for the interaction of neutrinos on hadrons can be written in terms of the quantities just defined as

$$\frac{d^2\sigma}{dQ^2 d\nu} = \frac{G^2 E'}{2\pi E} \beta \left\{ 1 - \frac{Q^2}{4EE'} + \frac{\nu^2 + Q^2}{2EE'} [(R) + (L)] + \frac{E+E'}{2EE'} \sqrt{\nu^2 + Q^2} [(L) - (R)] \right\} \quad (6)$$

where,

$$\beta = W_2 = \frac{1}{2\pi} \frac{Q^2}{\nu} \frac{1}{[1 + (Q^2/\nu^2)]} \left(1 - \frac{Q^2}{2M\nu} \right) (2\sigma_S + \sigma_R + \sigma_L) \quad , \quad (7)$$

$$(R) \equiv \frac{\sigma_R}{2\sigma_S + \sigma_R + \sigma_L} \quad , \quad (L) \equiv \frac{\sigma_L}{2\sigma_S + \sigma_R + \sigma_L} \quad , \quad (8)$$

where σ_R , σ_L and σ_S are cross sections for the appropriate helicity states.

For $Q^2 \ll \nu^2$ Eq. (6) becomes

$$\frac{d^2\sigma}{dQ^2 d\nu} = \frac{G^2 E'}{2\pi E} \beta \left[1 + \frac{\nu}{E'} (L) - \frac{\nu}{E} (R) \right] \quad (9)$$

$$\text{or } \frac{d^2\sigma}{dx dy} = \frac{G^2 M E}{\pi} \nu \beta \left[(1-y) + \frac{y^2}{2} [(R)+(L)] + y(1-\frac{y}{2}) [(L)-(R)] \right] \quad (10)$$

where

$$\nu \beta = \frac{Q^2}{2\pi} (1-x) (2\sigma_S + \sigma_R + \sigma_L) \quad (11)$$

and

$$x = Q^2/2M\nu \quad , \quad y = \nu/E \quad (12)$$

$$0 \leq x \leq 1 \quad \quad \quad 0 \leq y \leq 1$$

Some motivation for the use of the variable x can be seen if one supposes that the neutrino might scatter off only a fraction, x , of the nucleon. The kinematics of quasi-elastic scattering is obtained by replacing M by xM . It would be represented in Fig. 1 by a radial line from the origin with a slope x times that of the one for $Q^2 = 2M\nu$. Bjorken has shown that at high incident energies if the parts are point-like $Q^2 \cdot (\sigma_R, \sigma_L, \text{ and } \sigma_S)$ are functions of x only (scale invariance). When one integrates equation (10) over x and y one obtains $\sigma = (\text{constant}) \cdot E$, a relation that we can test experimentally provided we detect all final states. Multiplicities and the dependence on x and y will be measured and compared with the predictions of various models.

1. "Spin-1/2-Parton" Model

To obtain a feeling for where events would lie in the $Q^2 - \nu$ plane for the "spin-1/2-parton" model, we have set $\nu \beta = (\text{constant}) \cdot (1-x)$ and $\sigma_R = \sigma_S = 0$. Fig. 4 shows how 1000 50-GeV neutrino interactions would be distributed under these assumptions. The important point is that all sectors contain statistically significant populations.

2. Pomeranchukon-Exchange Model

Predictions for the Pomeranchukon-exchange model can be obtained by setting $\gamma\beta = (\text{constant})(1-x)$ and $\sigma_L = \sigma_R, \sigma_S = 0$. The distribution of 1000 events at 50 GeV for these assumptions are shown in Fig. 5.

We propose to make our detection efficiency high in all sectors of the Q^2 - vs - γ plot and consequently, to be able to measure the total cross section. Bjorken and Paschos⁹ point out that the difference $\sigma_\gamma - \sigma_{\bar{\gamma}}$ is very model dependent. We wish to expose the chamber to both γ and $\bar{\gamma}$.

3. Possible effects of an Intermediate Vector Boson (IVB) on Scaling.

The effects of an (IVB) would be to modify the differential distribution $d^2\sigma/dx dy$ of eq. 9 by the (IVB) propagator factor $[M_w^2/(Q^2 + M_w^2)]^2$. This would produce breakdown in "scaling". Such a factor is most easily detected experimentally for large energy transfers. Fig. 6 illustrates its detectability at $y=0.9$ for 20 and 50 GeV neutrinos by showing how the function $\gamma\beta = K(1-x)$ would be modified by an (IVB) of mass 8 GeV. It is imperative that we be able to identify the muons of low momentum that correspond to large y values. Fig. 3 shows us that we must place EMI detectors near 90 degrees in order to detect them. Very low momentum muons will be trapped in the chamber by the magnetic field.

B. Intermediate-Vector-Boson Decay Modes

Although the bubble chamber is best suited to studying the hadronic decay modes of the (IVB), it is also capable of identifying the leptonic decay modes. Calculations⁸ indicate that the μ^- associated with W^+ production has a reasonable chance of having a momentum less than 1 GeV/c. It then can be trapped in a circular orbit within the chamber and will identify itself by not interacting. The μ^+ from the $W^+ \rightarrow \mu^+ \nu$ decay will be emitted at much higher energy into the forward direction and will be detected with high efficiency in the EMI. In fact, scanning for these events (produced either

in a full chamber of Ne, H, or D) is particularly simple. The signature is a trapped μ^- . If the (IVB) Mass is 5 GeV we expect 3500 (300) of them in the wide band (narrow band) exposure; and 350 if the (IVB) Mass is 8 GeV.

C. Heavy Lepton Search

The identification of a muon in the EMI allows one to form the invariant mass of this muon with other detected particles such as photons and mesons. The existence of a heavy lepton that decays into these combinations would produce a peak in the invariant mass combination.

D. Lepton Locality

It has been shown¹³ that if the distribution in ϕ , the angle between the normals to the hadron plane and lepton plane, in reactions of the type

$$\nu p \rightarrow \mu^- p y^+$$

where y^+ is any meson system, is not given by

$$\frac{d\sigma}{d\phi} = a + b \sin \phi + c \cos \phi + d \sin 2\phi + e \cos 2\phi$$

then lepton locality is violated. Other things, (see Pais ref. 5) such as s-channel-helicity conservation, pomeron exchange, and V-A interference, can be tested with this distribution, which we propose to measure.

E. Exclusive Reactions

We will be able to study in detail several exclusive reactions. For example, consider

$$\nu p \rightarrow \mu^- (\Delta^{++} \rightarrow \pi^+ p)$$

with which the Adler condition relating the cross section at small θ_μ to that for $\pi^+ p \rightarrow \Delta^{++}$ can be tested. Other resonance production reactions can be more easily studied if one has muon identification. The invariant-mass plots will not have muons masquerading as hadrons.

F. Unusual Events

One should also be prepared for unusual and unexpected processes to occur. Hydrogen and, to a lesser degree, deuterium are the best target materials for uncovering such rare processes. Muon identification will help in bringing unusual events to our attention.

III. Yields

A. Narrow Band Beam

Nezrick⁶ has described a way of producing a narrow band beam (NB) of neutrinos with a magnetic horn. It essentially focusses 70 ± 4 GeV mesons emitted with angles between 3 and 12 milliradians to produce 27 ± 3 GeV neutrinos from pion decay, and 67 ± 4.5 GeV neutrinos from kaon decay. Other versions⁷ of NB beams use quadrupole magnets as focusing elements. It is not clear at this time which form will be most suitable for our purposes or which form NAL is going to develop. We shall use whatever is available.

Table I summarizes the meson yields and the number of neutrino interactions per 10^{19} interacting protons for two types of NB focusing devices, the first a Nezrick type Monohorn that accepts 100 ± 5 GeV mesons emitted between 2 and 8 milliradians, and the second a Quadrupole system that accepts 100 ± 5 GeV mesons between 0 and 4 milliradians. The latter is compared with the NAL-Cal Tech (Expt 21) system that has the same $\Delta p/p=0.1$ and has an aperture of 0 to 2 milliradians. Two meson production models are used, CKP,⁹ and a new multiperipheral model of Clifford Risk¹⁰ that fits all π^\pm , and K^+ production data within 30% including the recent Argonne-Bologna-Michigan ISR results¹⁶ at equivalent energies of 500 and 1100 GeV. Details of these calculations will be presented in a separate document.¹¹ Figure 7 shows the probability per meson of emitting a neutrino from the $\mu+\nu$ decay mode into the 30 m^3 NAL bubble chamber within one meter of the beam axis. The calculations are made for a drift length of 400 meters and a shield length of 1000 meters. Also shown is how the fractional full width of the neutrino energy spectrum increases as the meson momentum is increased. It shows that the energy resolution of the pion neutrino beam deteriorates rapidly for meson momenta above 100 GeV. Figure 8 is used

TABLE I
Narrow Band Event Rates

Device Type	Angular Acceptance (mrad)	Production Model	$\Delta p/p = \pm 0.1$ Meson Energy E ₀	Mesons per 10 ³ Int. protons	Neutrino Energy \pm HW@Base	Thousands of Neutrino Interactions per 10 ¹⁹ Interacting Protons	Thousands of Neutrino interactions per 10 ¹⁹ incident Protons on a one mean free path target. [†]	Thousands of pictures required to produce 5000 pion neutrino events. For 3x10 ¹³ incident protons per pulse.
Quad ↓ Horn	0<θ<4	CKP	π ⁺ 400 100	9.6	43 ^{±7}	9.4	4.5	370
	"	Risk		17.5		17.1	8.1	205
	* 0<θ<2	"		6.65		6.5	3.1	540
Horn ↓	2<θ<8	CKP		11.5		11.2	5.3	310
	"	Risk		20.2		19.7	9.4	180
Quad ↓ Horn	0<θ<4	CKP	π ⁻	4.8		4.7	2.2	750
	"	Risk		10.0		9.8	4.7	360
	0<θ<2	"		3.61		3.5	1.7	100
Horn	2<θ<8	CKP		5.73		5.6	2.7	630
	"	Risk		14.1		13.7	6.5	260
Quad ↓ Horn	0<θ<4	CKP	K ⁺	1.92	96 ^{±10}	1.64	.78	
	"	Risk		0.90		0.77	.37	
	0<θ<2	"		0.30		0.26	.12	
Horn	2<θ<8	CKP		2.29		1.96	.93	
	"	Risk		1.43		1.22	.58	

* The CKP yield for 0 to 2 mrad is 0.423 that for 0 to 4 mrad.

† Account has been taken of the effects of meson absorption and nucleon cascading in thick target according to the prescription of reference (12). To convert from "interacting" to "incident" we multiply the "interacting" column by $(\frac{dn}{dq} / \frac{dn}{dq})_{\text{thin target}} = 0.475$

to illustrate how the neutrino interaction rate varies with meson momentum. The CKP production model is used together with a Quadrupole system that has a meson angular acceptance of 0 to 4 milliradians. The neutrino cross section was assumed to be $\sigma = 0.8 E \text{ (GeV)} \times 10^{-38} \text{ cm}^2$. The K^+ flux was assumed to be 0.2 that of the μ^+ at each momentum. The dashed curves are a modified version of CKP to give an approximate upper limit to the K^+ yield. The Risk model serves to give a lower limit to the K^+ yield (the model is valid for $p/p(\text{max}) \leq 1/2$, and underestimates the cross section for lower values of this ratio). The neutrino event rates per interacting proton of table 1 have not accounted for meson absorption in the target. This has been studied in detail¹², and shows that a target thickness of one mean free path is optimum for energetic mesons. Fig. 9 shows how the thin target meson momentum spectrum is distorted by nucleon cascading and meson absorption in thick targets. Here, $q = (p=100 \text{ GeV})/[T_0=0.305(400 \text{ GeV})^{3/4}] = 3.65$, where, T_0 is one of the parameters of the CKP formula. Consequently, the yields should be diminished by the factor 0.475.

B. Wide Band Beam

Kang, Walker, et al¹⁴ have estimated that there will be about one event per picture when the 15-foot bubble chamber filled with hydrogen is exposed to the wide band neutrino beam produced by 400 GeV protons. This assumes a fiducial volume of 20 m³, 3×10^{13} interacting protons per pulse, ideal focussing (100%) and a linearly rising neutrino total cross section. The calculation is based on the Hagedorn-Ranft model extrapolated to 400 GeV.

For 50,000 events we need about 50,000 pictures. The expected energy distribution of these 50,000 events is given in Table II. We see that while the bulk of events will be below 60 GeV a significant number of events at higher energies will be obtained.

An attempt has been made to estimate the (ν_e) production yield expected with

the broad band beam using the cross sections per nucleon computed by Wu and Yang¹⁵ for a aluminum target and assuming they apply to hydrogen. This is given in Table III

TABLE II

Distribution of all events from 50,000 event exposure with 400 GeV broad-band beam, assuming

<u>E (GeV)</u>	<u>Events</u>
0-10	1,300
10-20	9,200
20-30	12,800
30-40	9,400
40-50	4,900
50-60	3,000
60-70	1,800
70-80	1,200
80-90	900
90-100	700
100-150	2,500
150-200	1,600
200-250	500

TABLE III

Expected production in broad band exposure with 50,000 total events using estimates of Wu and Yang¹⁵.

<u>Mass of IVB (GeV)</u>	<u>Events</u>
3	28,000
5	3,500
8	350
10	100
15	5

IV. Analysis

A. Narrow Band Beam Events

With the EMI and a somewhat ambiguous knowledge* of the neutrino energy it will be possible to determine the momentum transfer squared Q^2 , and the energy transfer, ν . With a large bubble chamber some of the final state hadrons will identify themselves by subsequent interaction in the hydrogen. In particular, we will do all we can in this regard to detect and identify the final nucleon. The EMI will be useful in identifying neutron stars by their lack of an outgoing muon.

B. Wide Band Beam Events

For high energy neutrino interactions we are beset with the problem of not being able to determine the neutrino energy. We shall adopt the following analysis procedure in order to obtain an approximation to the neutrino energy.

- 1) Measure the momenta of all charged tracks.
- 2) Identify the muon.
- 3) Identify as many other particles as possible.
- 4) Determine the transverse momentum of the missing neutral system.**
- 5) Set the energy of the neutral meson system equal to one half of the sum of the magnitude of the momenta of the charged mesons (but never less than the missing transverse momentum)
- 6) The approximate neutrino energy is the sum of the energies of all outgoing charged particles plus this assigned energy of the neutral system minus the proton rest mass.
- 7) Pray† and do some statistical type consistency tests.

* There are kaon and pion neutrinos in the beam.

** Those events that have no missing transverse momentum are candidates for "3c fit" class. For them E can be measured

† Replace 7) with a Phase I Quantameter as soon as possible (Proposal 9D to be submitted).

Actually, this procedure might work reasonably well for the average event. For example, suppose the muon receives $2/3$ of the initial neutrino energy. Of the remaining $1/3$ only $1/3$ will be energy of neutral particles. Therefore, $1/9$ of the energy would be missing. Results from the narrow band exposure will also help.

V. Experimental Equipment

The equipment required by this experiment may be summarized as follows:

1. external proton beam having an energy of around 400 GeV and an intensity of $2 \text{ or } 3 \times 10^{13}$ interacting protons per pulse,
2. neutrino beam facility consisting of a low Z target (1 mean free path thick), narrow-band and broad-band focusing systems, meson drift space, and muon shield,
3. neutrino beam monitors to determine the shape of the neutrino energy spectrum and to measure the neutrino flux during a given bubble chamber run,
4. NAL 30 m³ bubble chamber with liquid hydrogen filling,*
5. EMI to distinguish muons from hadrons produced when neutrinos interact in the bubble chamber.

Each of the items listed represents a major developmental effort with the total far exceeding the capabilities of any one group. It is important to us, nevertheless, to have a working knowledge of each of these facilities, and for this reason members of our collaboration have participated and will continue to participate in each phase of the NAL 30 m³ bubble chamber program.

Our main effort will, of course, be invested in the area of muon identification. The remainder of this section contains a brief description of the EMI and indicates how it will be used to improve our understanding of the physics of neutrino interactions. A more detailed description is given in NAL Proposal 9C.

A preliminary sketch of the complete EMI geometry is shown in Figure 10a and 10b. The complete EMI consists of: 1) a passive internal absorber filling the space between the magnet coils and matching the coil thickness in collision lengths (3.2 collision lengths stainless steel subtending approximately 180° horizontally and weighing 20 tons); 2) an active detector-absorber-detector

* Requests for deuterium and neon filling will be deferred until more is known about the bubble chamber operation.

sandwich (3 collision lengths stainless steel subtending 60° vertically and nearly 180° horizontally and weighing 111 tons. The "Phase I EMI"³ will consist of the passive internal absorber and a single detector plane. The detector planes will be multi-wire proportional chambers with x, y, and diagonal position information in each plane.

The vertical distribution of muons at a radius of $R = 3.2$ meters measured from the center of the bubble chamber is shown in Fig. 11 for 10-GeV neutrinos incident. This distribution was obtained from Monte Carlo calculations and is similar for both the Parton and Pomeronchuk-Exchange models. Less than 10% of the muons are outside ± 2 meters. The EMI shown in Fig. 10 is centered at a radius of 3.5 meters and has a total height of 5 meters, assuring 90% efficiency at 10 GeV.

The horizontal distribution at $R = 3.2$ meters is strongly influenced by the magnetic field. This is apparent in Fig. 12 where the spread in horizontal coordinates is given for various incident neutrino energies. An acceptance of $\pm 90^\circ$ will work well at 10 GeV and will be of some use down to 2 GeV. The geometric efficiency versus energy is plotted in Fig. 13 for an EMI with horizontal acceptance of $\pm 90^\circ$ and a vertical acceptance of $\pm 30^\circ$, essentially the geometry shown in Fig. 10a, b. Fig. 3 has already shown in detail (i.e. in terms of x and y) how the muons from 20 GeV neutrinos are swept out by the bubble chamber magnetic field.

The geometric efficiency provides an indication primarily of what fraction of the muons are subject to particle identification. By extrapolating the individual tracks observed in the bubble chamber, it will be possible to determine which tracks may be identified.

Mesons and hadrons are distinguished in the EMI by requiring that all hadrons interact. No attempt is made to stop hadrons or to absorb the total hadron energy with good efficiency. Incident hadrons thus manifest themselves through track displacements indicating a large-angle scattering, through

hadronic cascades of multiplicity greater than unity, and through total absorption.

Experimental tests have been carried out at the Lawrence Berkeley Laboratory to determine the efficiency for rejecting pions in a muon identifier consisting of proportional chambers interspersed with iron absorber.³ Some preliminary results from these tests are plotted in Fig. 14, which gives the fraction of the pions surviving (i.e., not yet distinguished from muons) versus the thickness of iron absorber.

A surviving pion is defined in these tests as an incident beam particle that passes through the absorber and produces a single track within the multiple-scattering envelope containing a given fraction of the incident muons. In the actual bubble-chamber experiment, particle trajectories will be determined by measuring individual tracks observed in the bubble chamber and by extrapolating these tracks out to the external detectors. The radius of the multiple-scattering envelope containing 96% of the muons is approximately 3 cm for 4 GeV particles at the first EMI detector plane, thus the accuracy required in the extrapolation is modest.

Fig. 14 implies that the Phase I EMI, consisting of internal passive absorber plus hydrogen plus vacuum walls (3.9 collision lengths = 30 cm iron equivalent), will reject $(94 \pm 1)\%$ of the pions while accepting 96% of all muons. A more complete EMI, with an additional 3 collision lengths of stainless steel (6.9 collision lengths = 89 cm iron equivalent) will reject $(98.5 \pm 1)\%$ of the pions while accepting 96% of all muons. For the complete EMI with two MWPC planes the pion rejection is estimated to be 99.5%.* As indicated previously, the Phase I EMI, with 94% pion rejection, is adequate for this proposal.

* Tests are continuing to verify this estimate.

For this present proposal, we plan tentatively to use the Phase I EMI. Clearly, if a more complete version of the EMI is available before the bubble chamber is operational, we would use this version. The EMI tests suggest that a single detector plane may be adequate for the complete EMI, in which case it may be relatively simple to go from a Phase I EMI to the complete model.

VI. Schedule and Participation

The time schedule for this experiment is related primarily to the date of successful operation of (a) the 15-foot bubble chamber filled with hydrogen and (b) the Phase I EMI. We assume target dates of January 1973 for both devices to be ready for experiments.

Prior to January 1973, the members of the UH-LBL collaboration will be heavily committed to the development and construction of the Phase I EMI (see Proposal 9C). This device will become an NAL facility for use with the bubble-chamber. At least one member of our collaboration is expected to be resident full-time during 1972 and until the EMI is fully working. Field tests of the prototype-EMI (by itself) and the Phase I-EMI (with the 15-foot bubble chamber) are essential to this program and will be conducted by this team at NAL. Thus, members of this collaboration should be quite familiar with the neutrino beam and bubble-chamber operation by January 1973.

Certain members of the UH-LBL collaboration are prepared to assist NAL, as needed, in the development of bubble-chamber track reconstruction computer programs. We are especially interested in the extrapolation of bubble-chamber tracks outward to the EMI detector-planes, since muon identification depends in part on the accuracy of the prediction of where the muon would hit the EMI.

Although others may be primarily responsible for development of a suitable narrow-band neutrino beam for bubble-chamber use (e.g., a narrow-band "horn", or a DC focusing device, e.g. quadrupoles), we wish to make use of such a facility and would be willing to assist in its development. We are particularly interested in focusing pions (and kaons) below 100 GeV, since the pion neutrino spectrum becomes too broad at higher energies. The narrow band pulsed horn, with predicted properties as described by Mezrick⁶, appears to us to be promising for our application, although pulsed Quadrupoles of large aperture

($\theta < 4$ mr) are also a possibility.

In anticipation of doing experiments with the NAL 15-foot chamber, both the LBL and Hawaii groups have been preparing bubble-chamber track measuring devices suitable for low contrast (i.e., Scotchlite illuminated) film. In particular, the Hawaii group is acquiring a "SWEEPNIK" laser-beam measuring machine which successfully measures events from similar film.

The coordinated analysis of neutrino events occurring in the hydrogen bubble-chamber with muons detected externally in the EMI will be developed by our group (see Proposal 9C). Many EMI events per pulse are expected, so that matching to the bubble-chamber event is required. A computer program which inputs bubble-chamber data and matches to the EMI stored-data is needed.

These various projects are all related to this basic physics proposal for studying neutrino interactions in hydrogen. The authors of this proposal anticipate spending most of their available research time on EMI development and related projects up to the operation of the NAL 15-foot chamber and EMI in early 1973. We believe that the EMI (muon identification of most neutrino events) will greatly enhance the physics value of the bubble-chamber for neutrino physics. We are committed to establish the EMI as a working facility and test it with the bubble chamber by a short exposure aimed at instrumentation (Proposal 9C). This proposal (9B) is a "physics" proposal using the EMI.

We propose the following experimental runs:

50,000 wide band neutrino events (50,000 pictures)

5,000 narrow band neutrino events from a 100 ± 5 GeV meson beam (180,000 pictures)*

5,000 narrow band anti-neutrino events from a 100 ± 5 GeV meson beam
(260,000 pictures)

* Calculated assuming 3×10^{13} 400 GeV protons incident on a one-mean-free path target followed by a Neuzrick type Monohorn ($2 < \theta < 8$ mr), using the Risk Multiperipheral production model (See the boxed items of Table I)

It is probable that in order to test the mechanism that is causing breakdown in scaling we will run part of the NB exposure at different energies. The results of the counter neutrino experiments will determine the optimum energies. The order in which the narrow band or wide band exposures take place and the number of pictures required depend on factors that are unpredictable at the moment. We expect that our "instrumentation" analysis of the 10^4 events of proposal 9C will be well enough along by September 1973 that we would be ready at that time to begin the "Physics" exposures of the present proposal. Requests for exposure to deuterium and Neon will be deferred until more is known about the bubble chamber operation.

REFERENCES

1. University of Hawaii, Northwestern University, and University of California, Lawrence Radiation Laboratory, "Proposal for a High Energy Neutrino Experiment in the NAL 30 m³ H₂, D₂ Bubble Chamber," NAL Proposal #9 (June 1970). (See also M.L. Stevenson "Neutrino Physics with Large H₂ Chambers", Proceedings of International Conference on Bubble Chamber Technology, pp. 56-122 (1970).)
2. A prototype quantameter has been successfully tested during the last year. Results of these tests will be published and are described in part in the following documents: "Delta Rays and the Proportional Quantometer," D. Yount, HEPG Report No. UH-511-92-71, February 8, 1971; "Multiwire Proportional Chambers with uniform Gain," S. Parker et al., submitted to Nucl.Instr. & Methods June 10, 1971.
3. The EMI and related tests are described in detail in NAL Proposal No. 9C "Proposal to Develop a Phase I External Muon Identifier (EMI) for use with the 30 m³ Bubble Chamber," University of Hawaii and University of California Lawrence Radiation Laboratory (July 1971), and supporting documents.
4. The percentage of high energy neutrinos has been enhanced in the latest beam design due to the long meson drift space (400 m) and muon shield (1000 m). It is in the high energy region that the EMI is expected to be of greatest usefulness.
5. J.D. Bjorken and E.A. Paschos, SLAC-PUB 678 December 1969 (Lectures by Bjorken at 1969 Summer Study). See also the excellent reviews of A. Pais "Weak Interactions at High Energies" Conference of "Expectations for Particle Reactions at the New Accelerators," University of Wisconsin (1970) and C.H. Llewelyn Smith. "Neutrino Reactions at Accelerator Energies" SLAC.

references 2

6. Frank A. Nezrick, "A Monoenergetic Neutrino Beam Using Current-Sheet Focusing Elements" 1971 National Particle Accelerator Conference, Chicago 1-3 March 1971, IEEE Transactions on Nuclear Science.
7. D. Keefe, UCRL 16830 p. 311, 1966.
V.Z. Peterson UCRL 16830 p. 324, 1966.
F. Sciulli, B. Barish, W. Ford, T. Oddone, C. Peck, A. Maschke, NAL Proposal No. 21, 1970.
8. R.W. Brown, R.H. Hobbs, and J. Smith (to be published). See also D. Cline, A.K. Mann, and C. Rubbia, Phys. Rev. Letters 25, 1309 (1971) and M.L. Stevenson, "High Energy Neutrino Physics ($E > 20$ GeV) and the Constraints Placed on the Detectors," 1969 NAL Summer Study, Vol. 2, 121 (1969).
9. G. Cocconi, L.J. Koester, D.H. Perkins UCRL 10022 (1961) p. 167 (1961 High Energy Physics Study, Summer 1961).
10. Clifford Risk (private communication) and C. Risk and J.H. Friedman UCRL 20199 "Comparison of an inclusive Multiphenal Model to Secondary Spectra in p-p Collisions."
11. Clifford Risk and M. Lynn Stevenson, Predicted Neutrino Fluxes for Ideal Narrow Band Systems. TM 318
12. M.L. Stevenson, "Targets for the Neutrino Beam: Concepts" Nal report TM-218.
13. A. Pais, Phys. Rev. Letters 9, 117 (1962); T.D. Lee, C.N. Yang, Phys. Rev. 126, 2239 (1962).
14. Y.W. Kang, J.K. Walker et al, NAL Report EM-265 (1970).
15. A.C.T. Wu, Yang, private communication.
16. L.G. Ratner, R.J. Ellis, G. Vannini, B.A. Babcock, A.D. Krisch, and J.B. Roberts, Phys. Rev. Letters 27, 68 (1971)

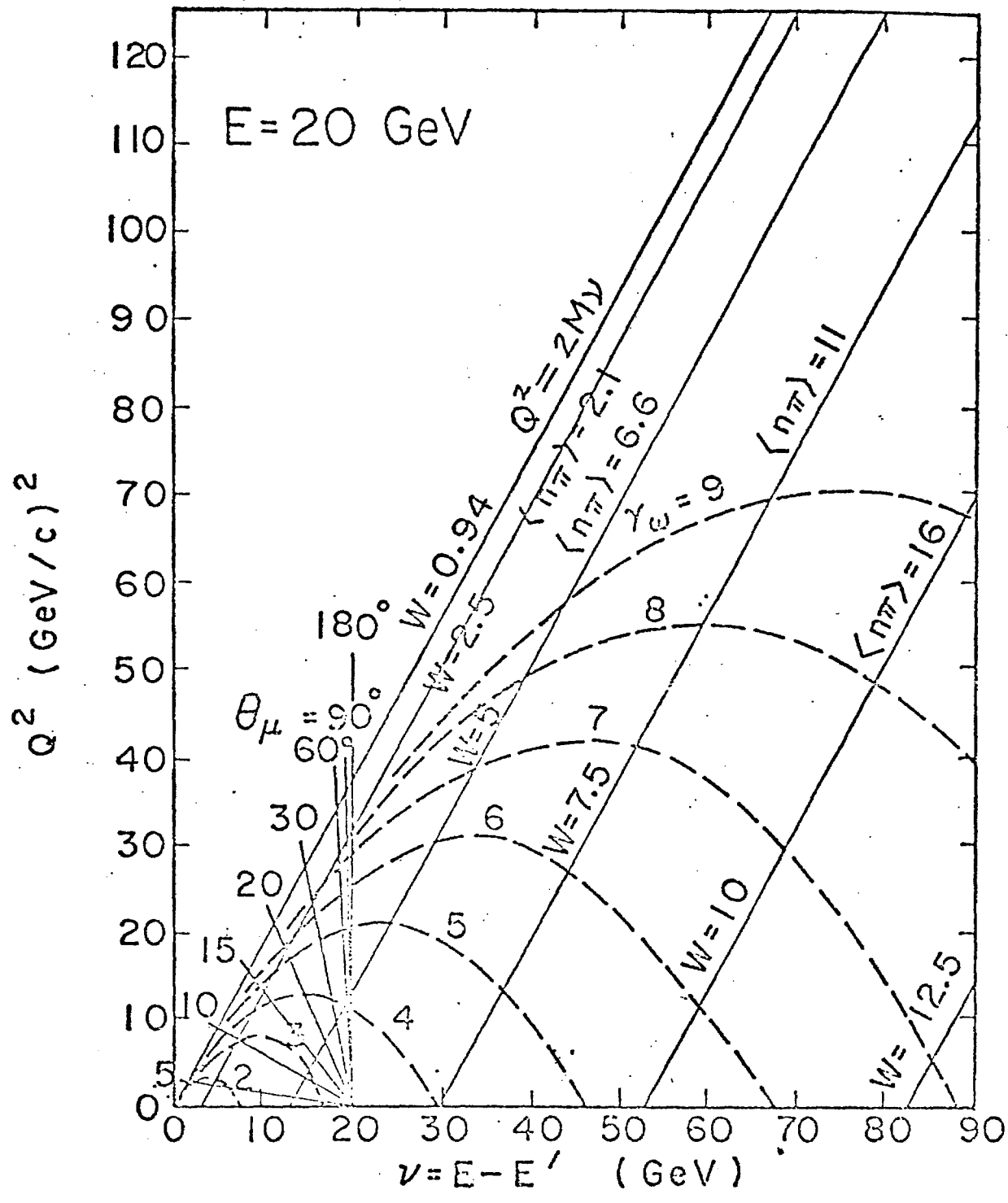
FIGURE CAPTIONS

9B-24

1. Summary of the Kinematics of $\nu + N \rightarrow \text{lepton} + \text{hadrons}$. Lepton Momentum Transfer Squared vs lepton Energy transfer. The parallel solid lines are loci of equal invariant hadron mass. On each line is given an estimate of the maximum pion multiplicity expected for such a mass. The dashed parabolic curves are loci of equal Lorentz contraction factors, γ_W , of the hadron system. The radial straight lines emerging from the point ($Q^2=0, \nu = 20 \text{ GeV}$) are loci of equal lepton laboratory angle for an incident neutrino of 20 GeV.
2. Summary of 20 GeV neutrino event configuration for various values of $x (\equiv Q^2/2M\nu)$ and $y (\equiv E-E'/E)$. The arrow gives the muon momentum and the cones illustrate where the hadrons might go.
3. Summary of how the muons from 20 GeV neutrino interactions are bent by the bubble chamber magnetic field.
4. Distribution of 1000 events predicted by a "spin-1/2-parton" model where $\nu\beta$ is chosen to be a constant times $(1-x)$. $\sigma_R = \sigma_S = 0$.
5. Distribution of 1000 events predicted by the Pomeron exchange model where $\nu\beta$ is chosen to be a constant times $(1-x)$. $\sigma_L = \sigma_R$ and $\sigma_S = 0$.
6. Examples of how "scaling" might be broken by an intermediate vector boson of MASS 8 GeV for 20 and 50 GeV neutrinos
7. Summary of the probability of decay neutrinos from monoenergetic pions and kaons passing through the central 1 meter radius of the bubble chamber. The meson drift length is 400 meters. The muon shield is 1000 meters. Also shown is the fraction full width (at the base) of the neutrino energy spectrum.

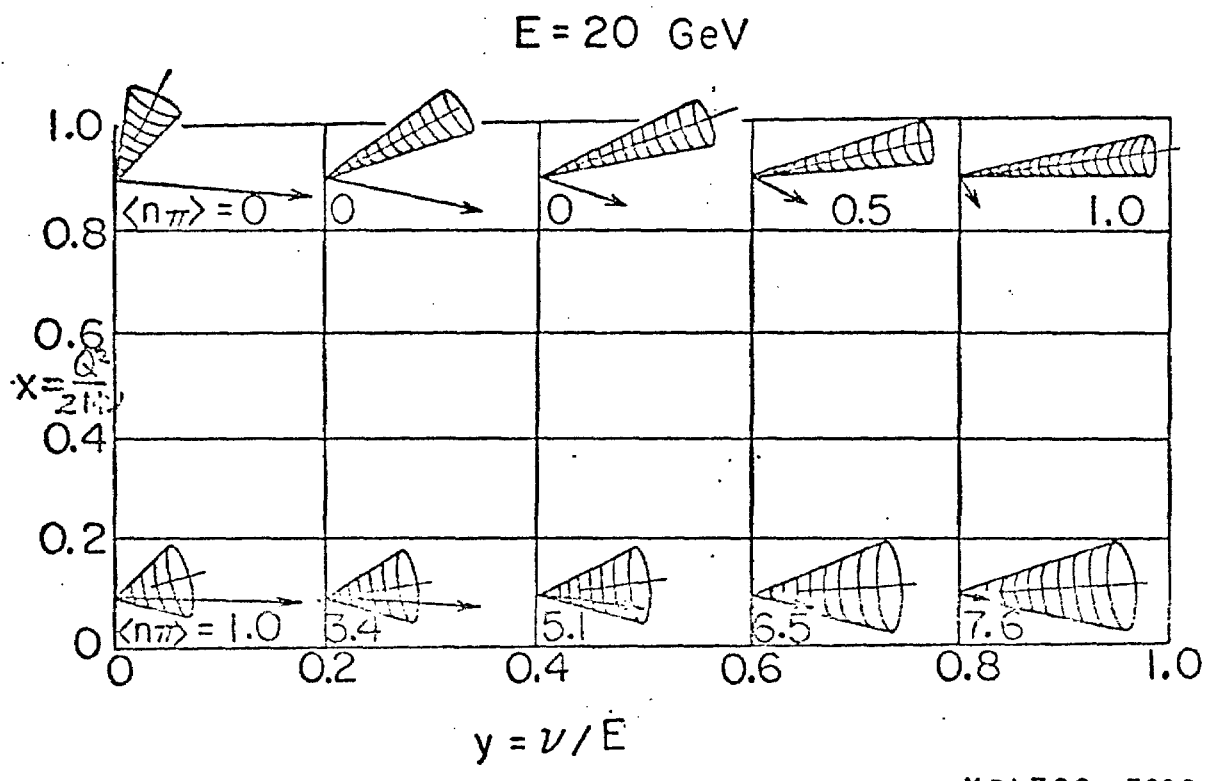
figure captions 2

8. The number of narrow-band neutrino interactions within one meter of the beam axis per 10^{19} interacting protons as a function of the momentum of the meson beam ($\Delta p/p = 0.1$). The upper horizontal scales summarize the corresponding neutrino energies for pions and kaons.
9. These curves summarize how nucleon cascading and meson absorption in targets of various thicknesses distort the "primary" or "thin target" meson production spectrum. For a target of one-mean-free path thickness the yield of 100 GeV mesons produced by 400 GeV protons will be diminished by the factor 0.475.
10. The full external muon identifier (EMI). The Phase I EMI will consist of only one plane of multi-wire proportion chambers.
11. Vertical distribution of 10 GeV muons at the first detector plane.
12. Horizontal distribution of muons at the first detector plane.
13. Geometrical efficiency of the EMI as a function of neutrino energy.
14. Fraction of pions that survive as a function of absorber thickness.



XBL709-3904

Fig. 1



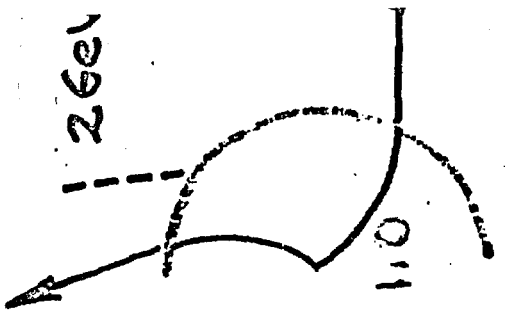
XBL709 - 3896

FIG. 2

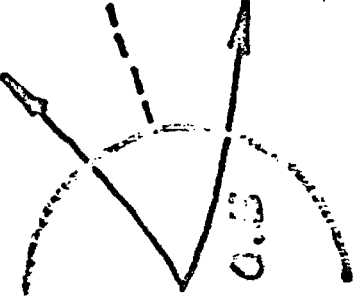
Muon Trajectories

$E = 206 \text{ GeV}$

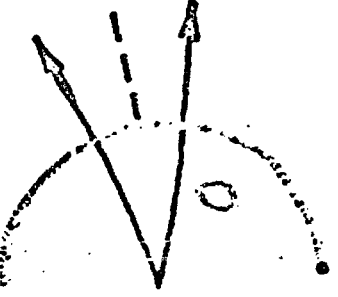
$E_{\mu} = 18 \text{ GeV}$



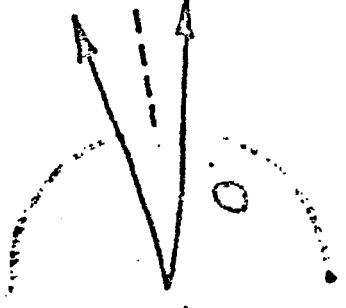
6 GeV



10 GeV



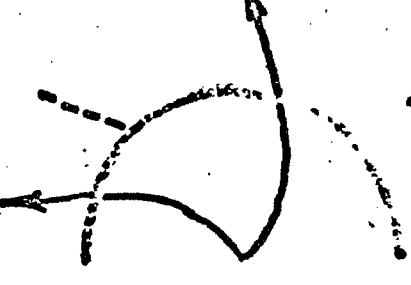
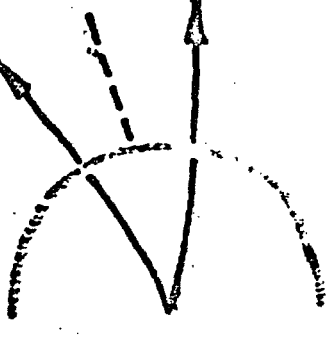
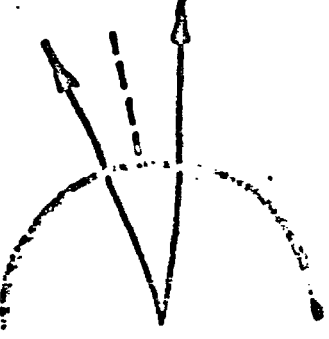
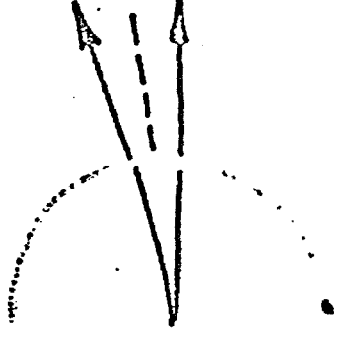
14 GeV



$x=0.9$

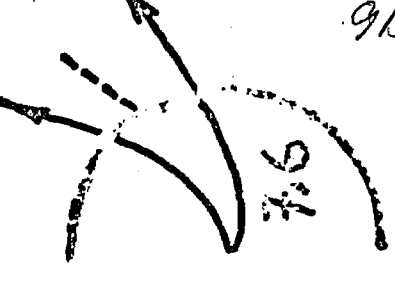
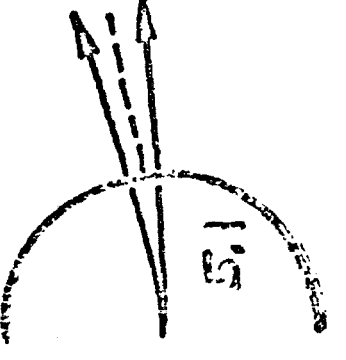
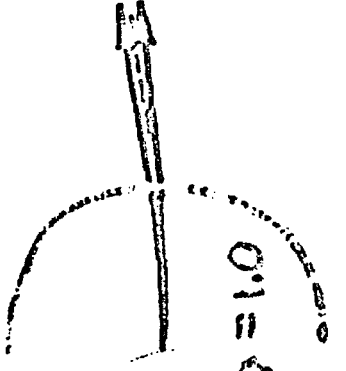
$x \equiv Q^2/2M_V$

$x=0.5$



$x=0.1$

$\langle \sin^2 \theta \rangle = 1.0$



0.5

0.7

0.9

$y \equiv \frac{E-E'}{E}$

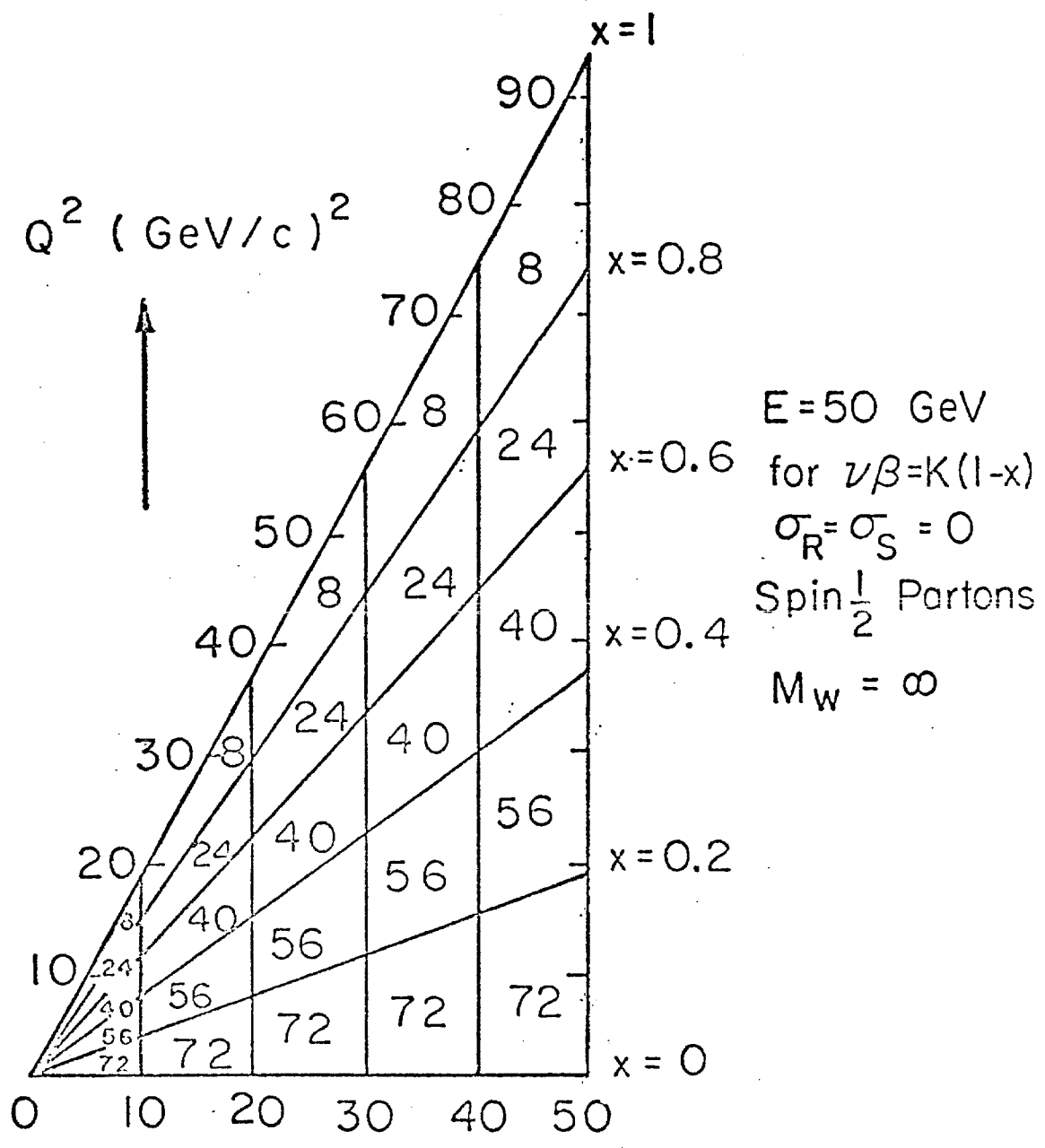
0.3

0.1

FIG. 3

913-78-1

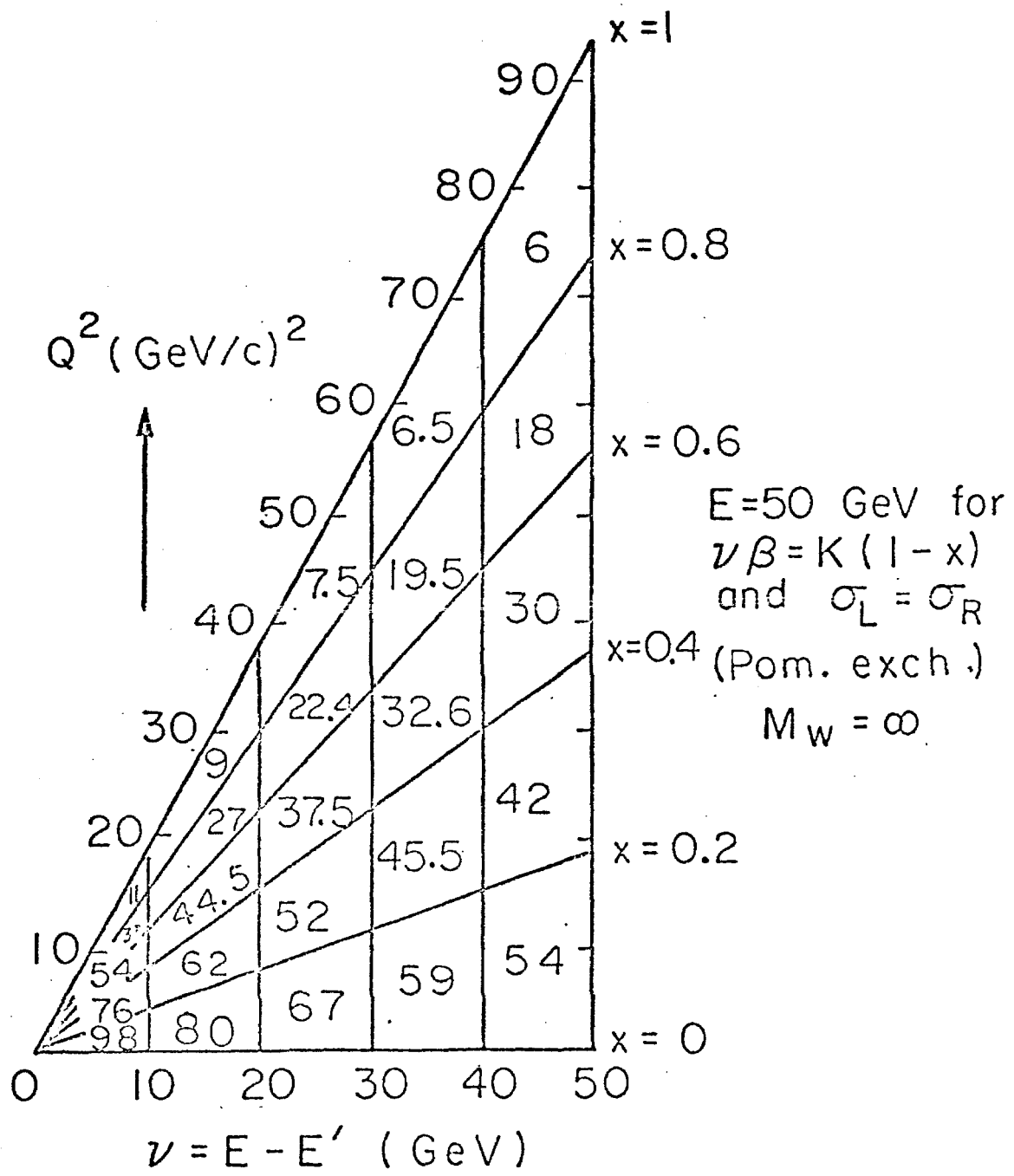
Distribution of 1000 events



XBL709-3893

FIG.4

Distribution of 1000 events



XBL 709-3894

FIG.5

Modification of Scaling with W Propagator

9B-31

for $M_W = 86 \text{ GeV}$

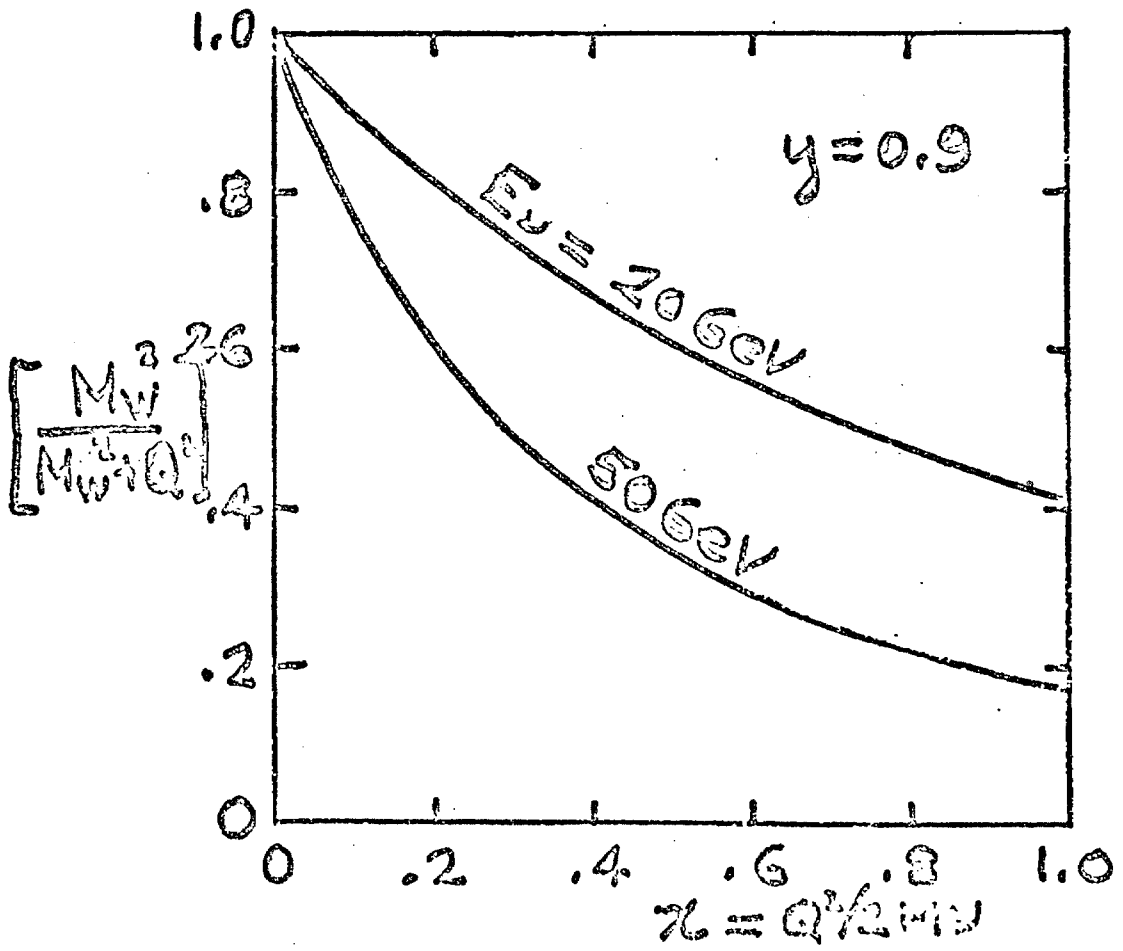
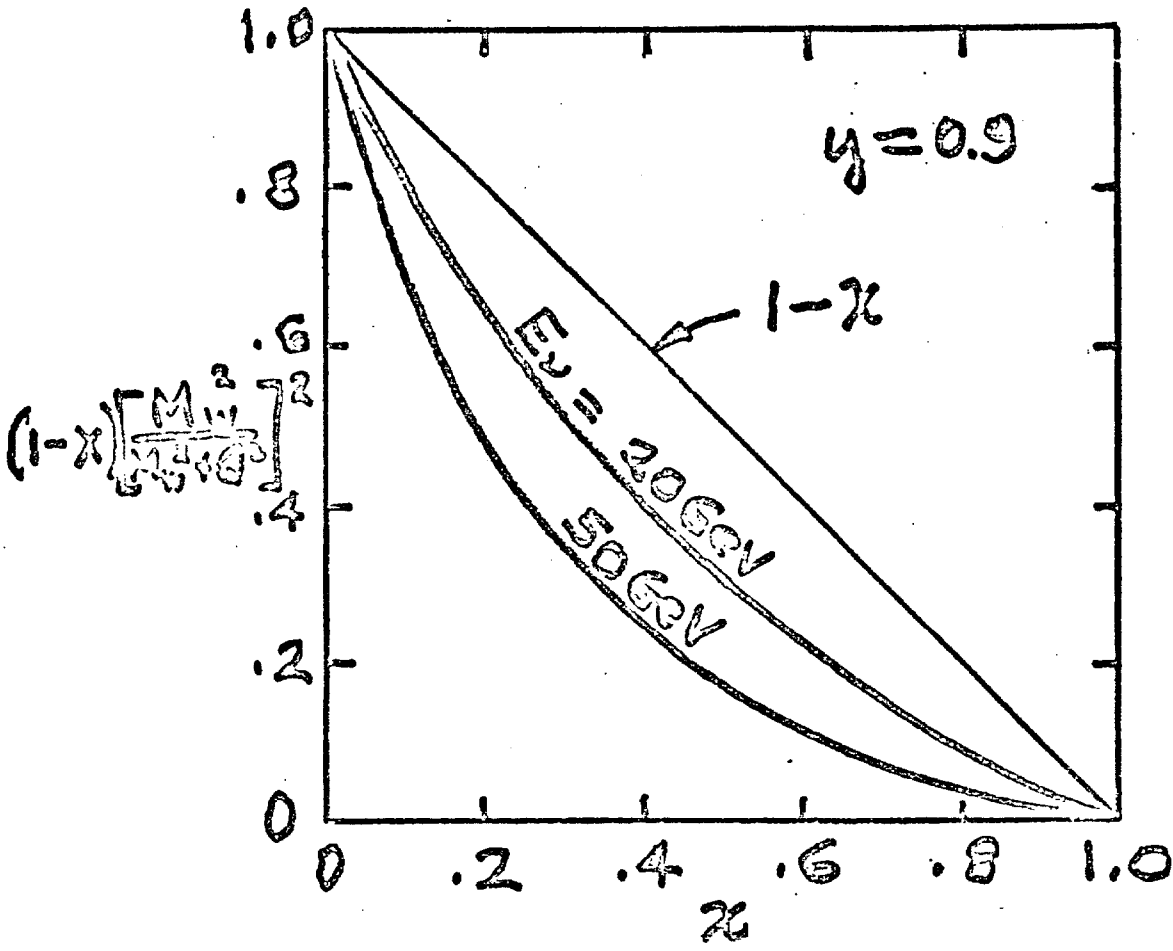


FIG. 6

Number of Maximum Interactions / 10^{19} Interacting p-p's

$N_1(\text{GeV})$ 20 30 40 50 60 70

$N_2(\text{GeV})$ 40 60 80 100 120 140 160

(Number of Maximum Interactions)

Meson Momentum (GeV/c) 50 100 150

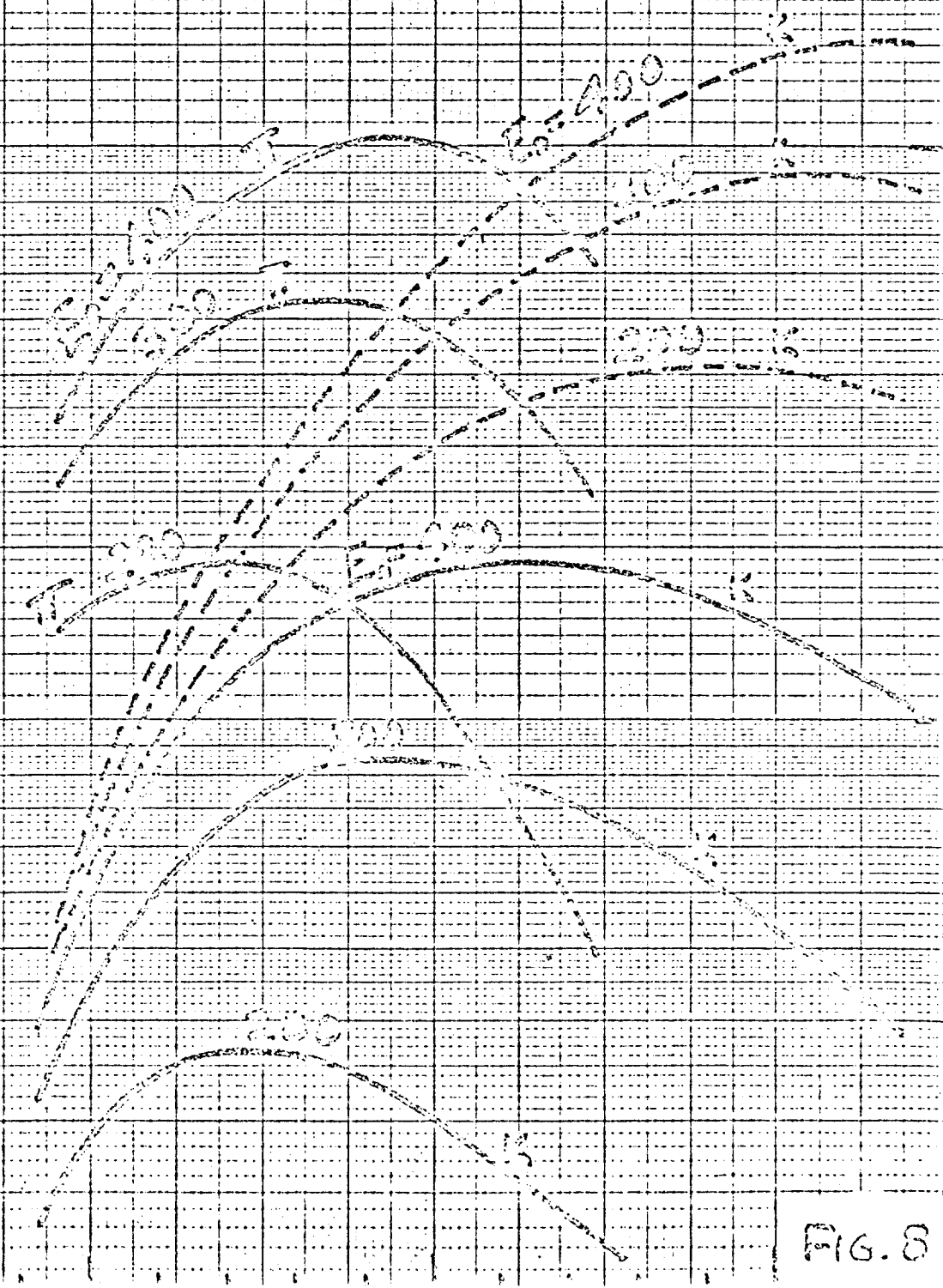


FIG. 8

$$b \equiv \frac{e^{-3Kq/4} - \beta \left(1 - \frac{\lambda}{\lambda_{\pi}}\right)}{\beta^2}$$

$$\lambda_{\pi} = \lambda$$

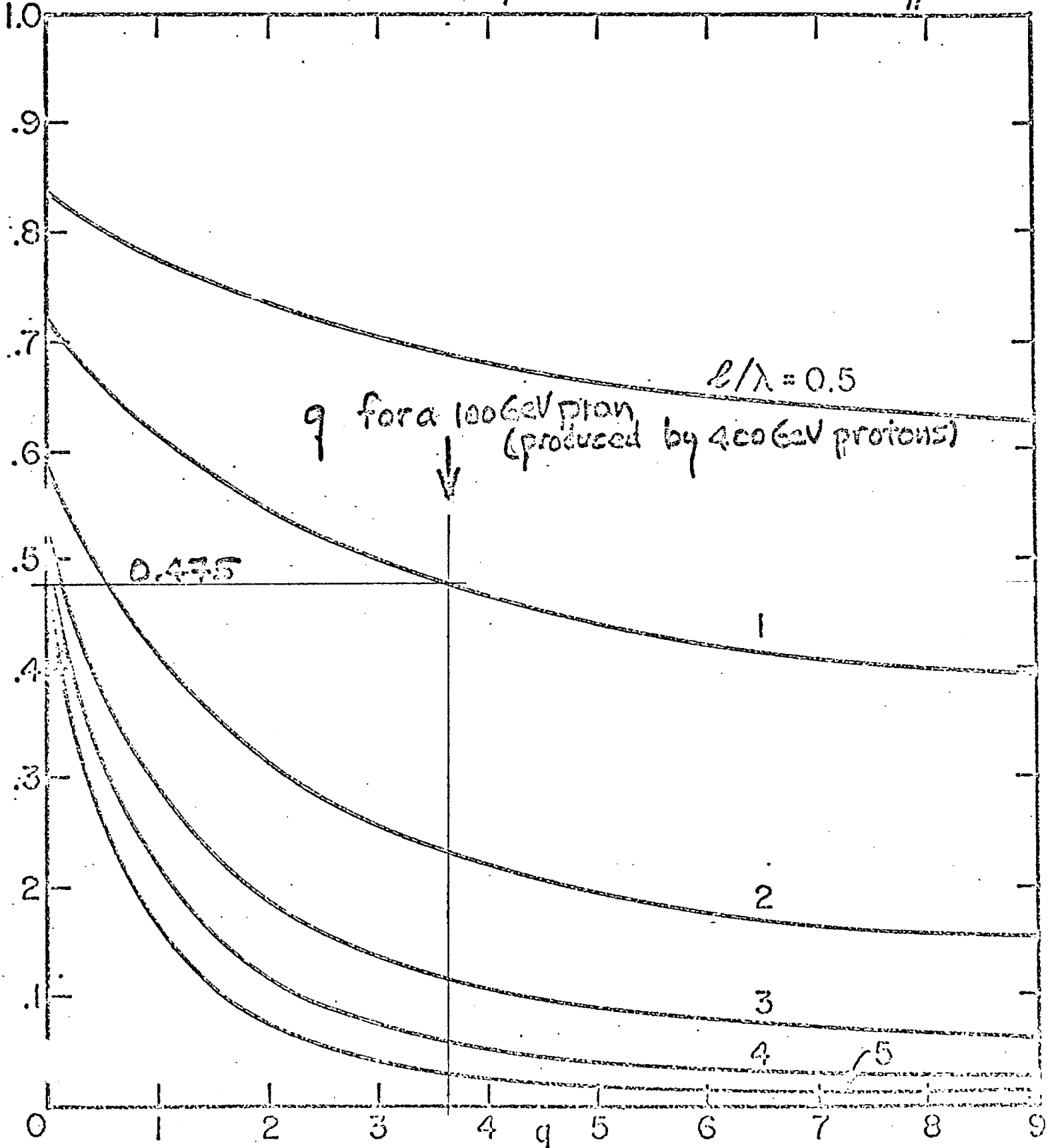


FIG. 9

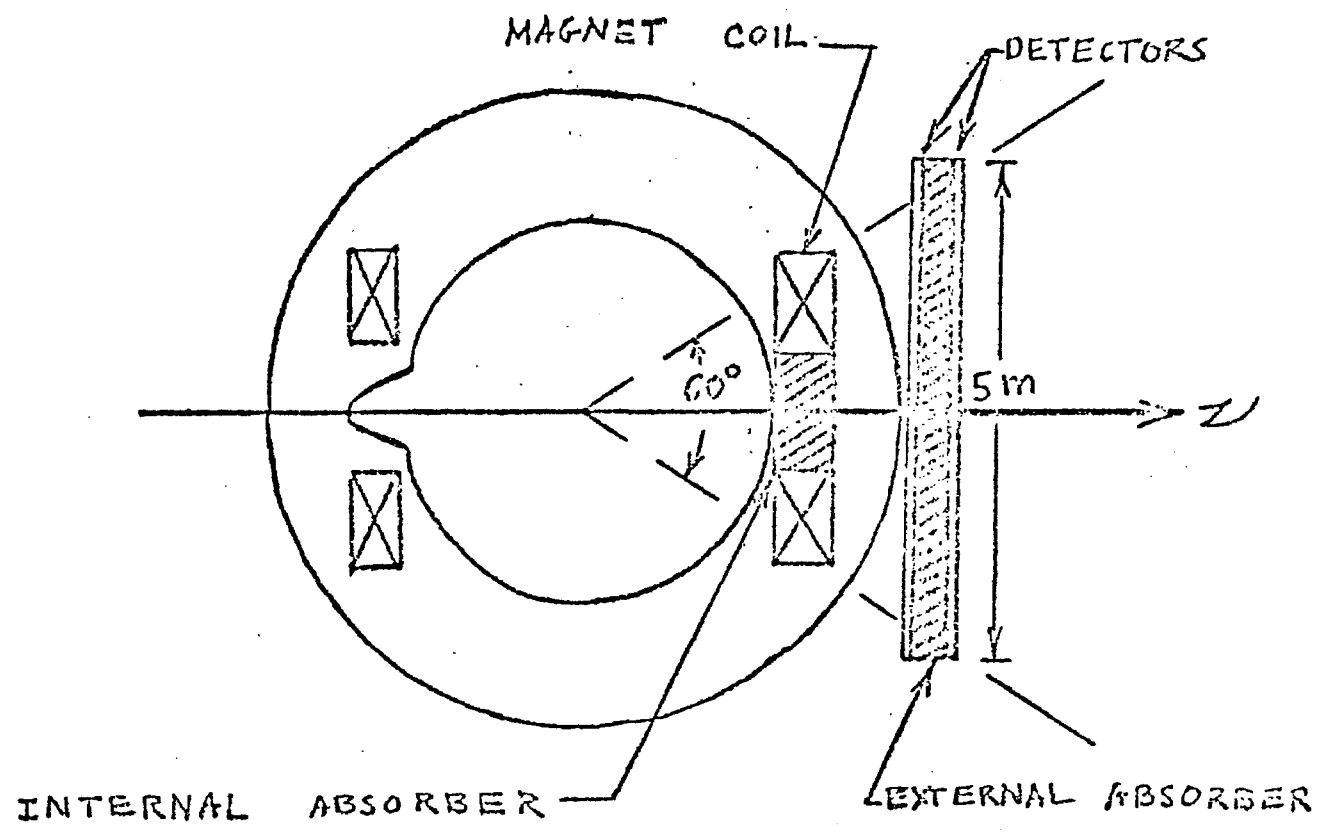


Fig. 10 a BUBBLE CHAMBER AND EMI, SIDE VIEW

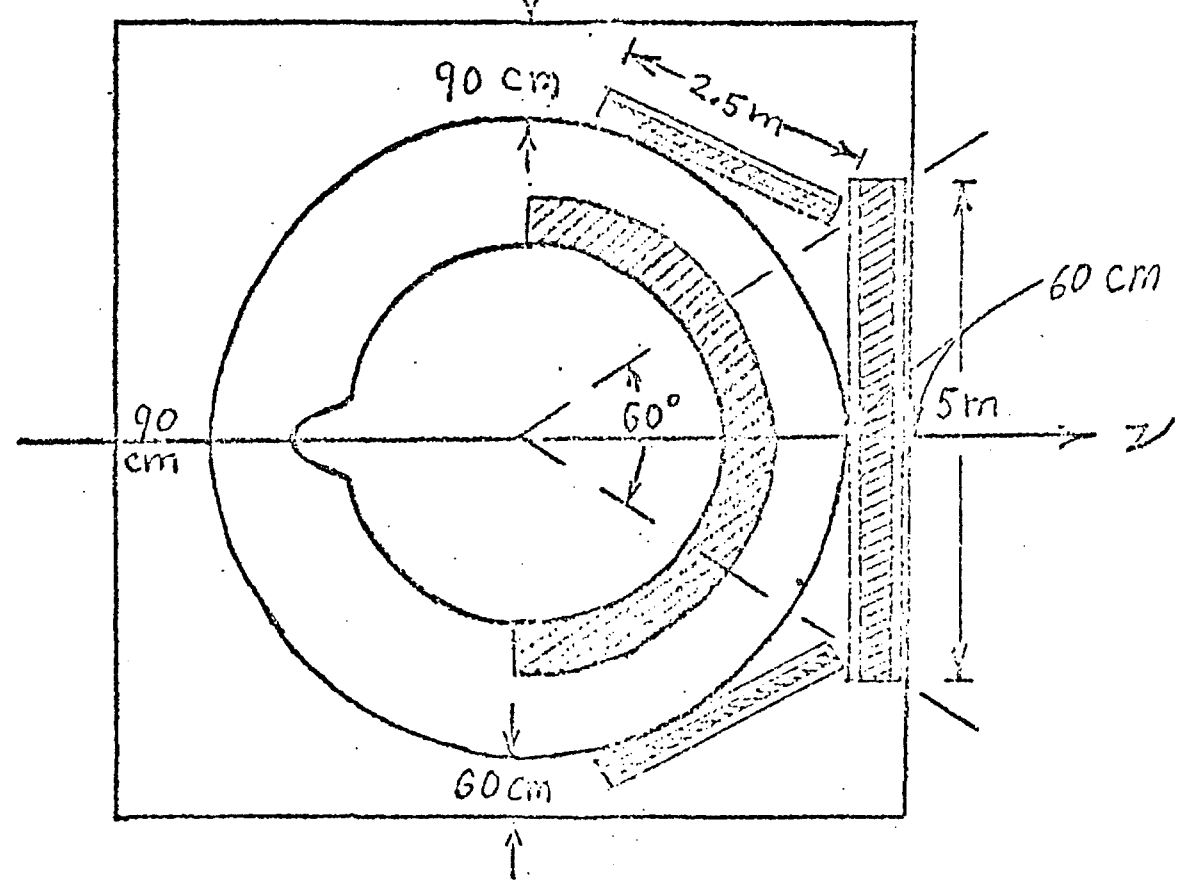
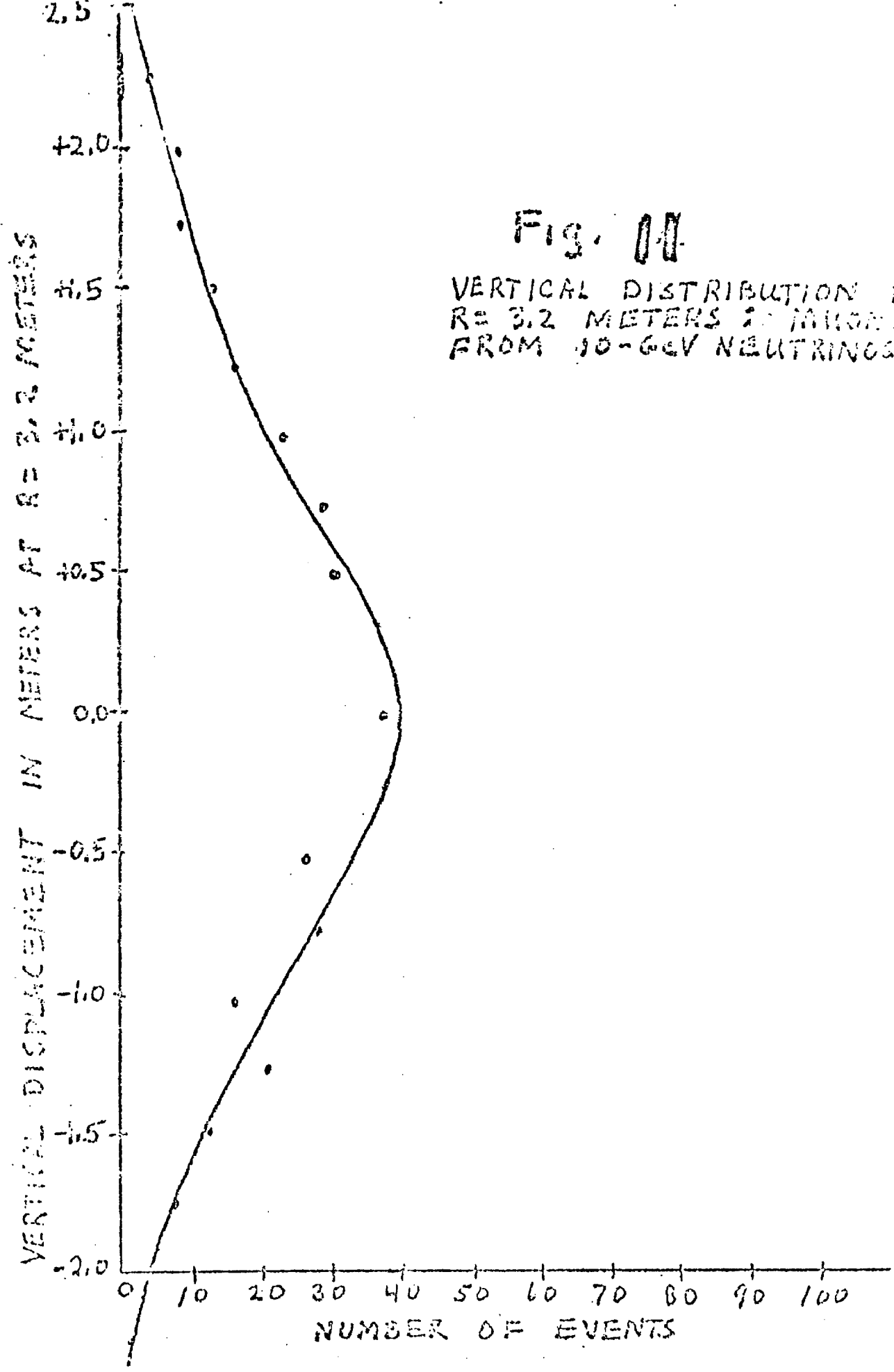


Fig. 10 b BUBBLE CHAMBER AND EMI, PLAN VIEW

Fig. 00

VERTICAL DISTRIBUTION AT
R = 3.2 METERS 20 MILES
FROM 10-GeV NEUTRINOS



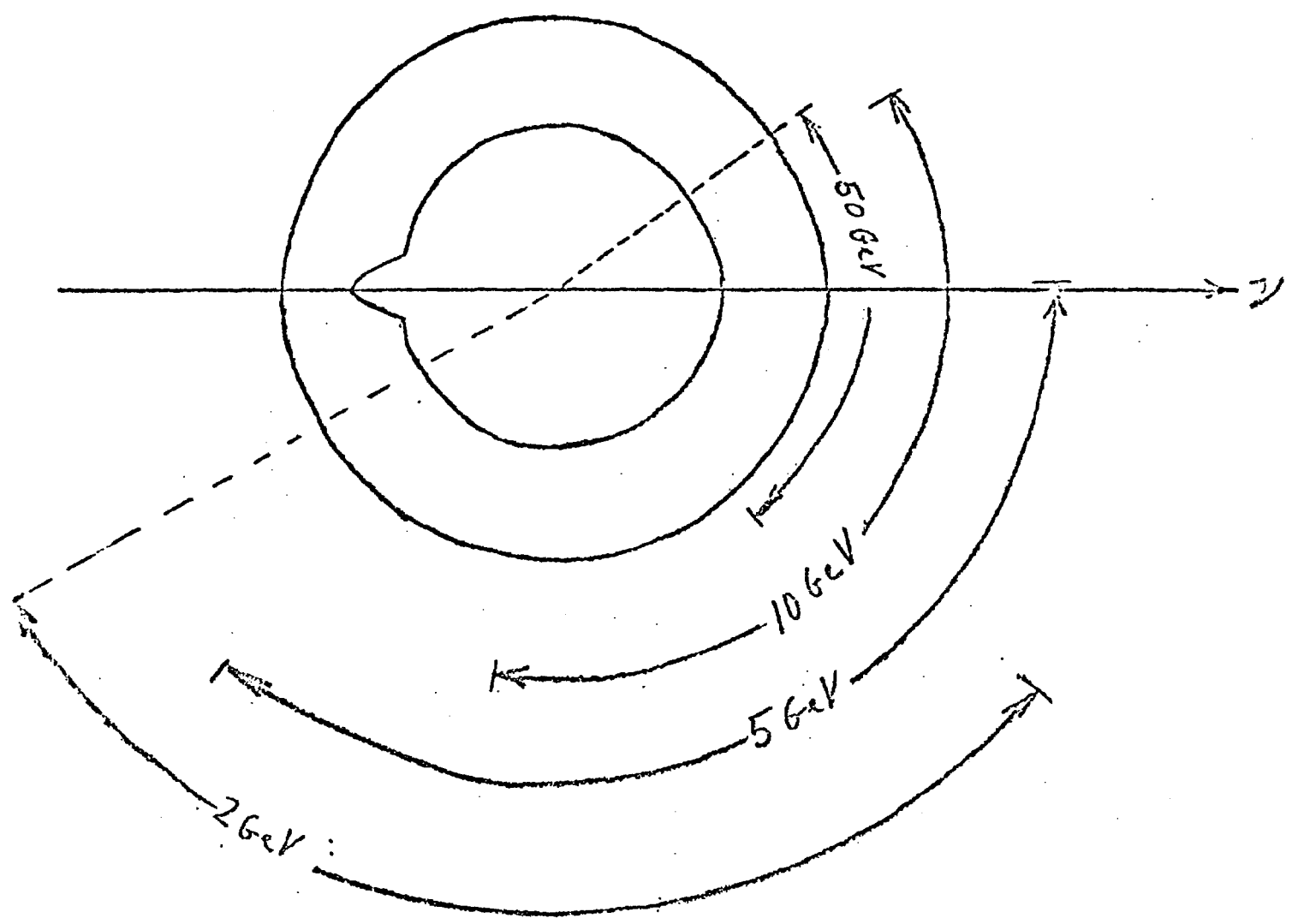


Fig. 12 HORIZONTAL DISTRIBUTION OF MUONS AT R=3.2 METERS

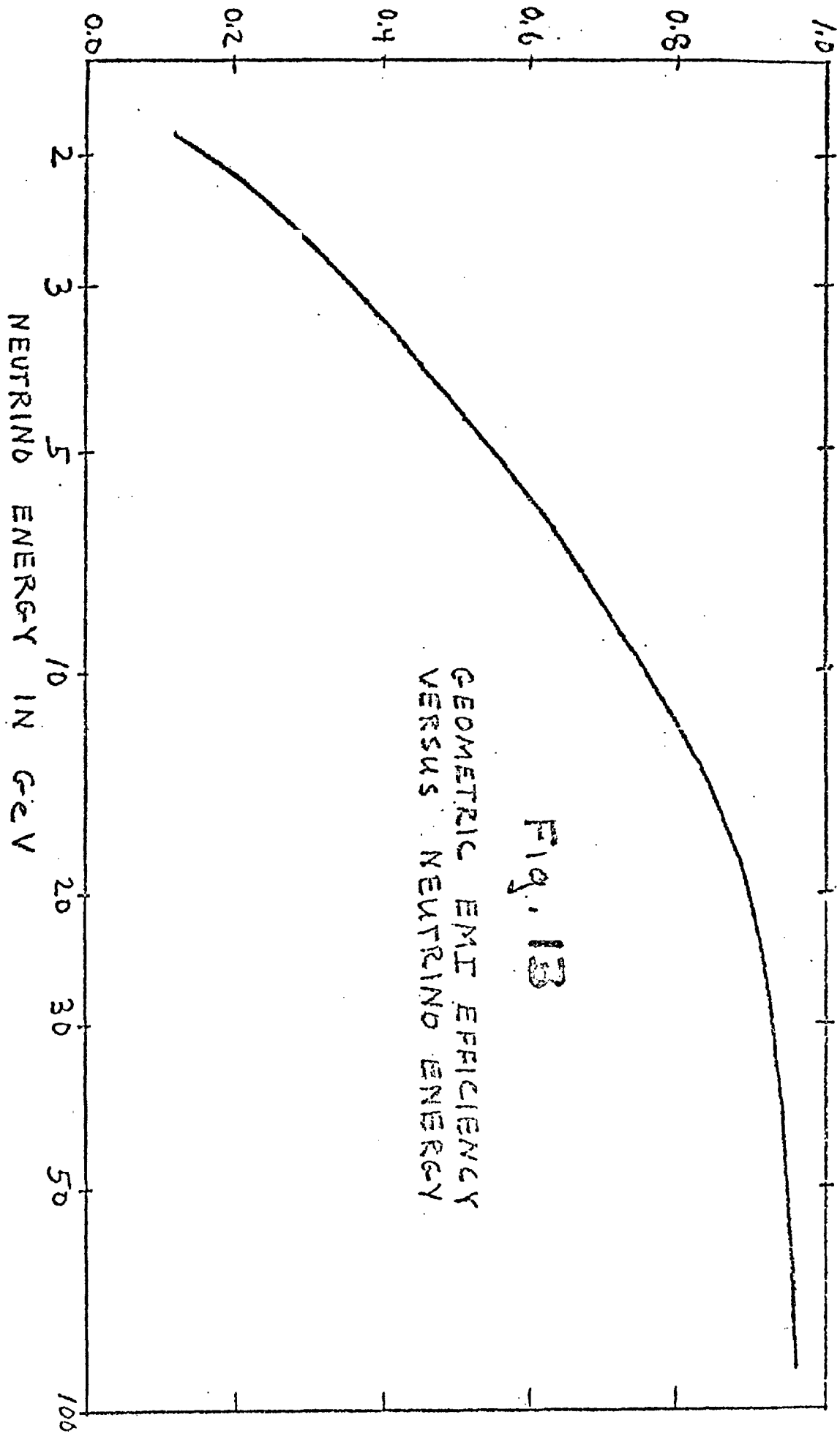


Fig. 13
GEOMETRIC EMI EFFICIENCY
VERSUS NEUTRINO ENERGY

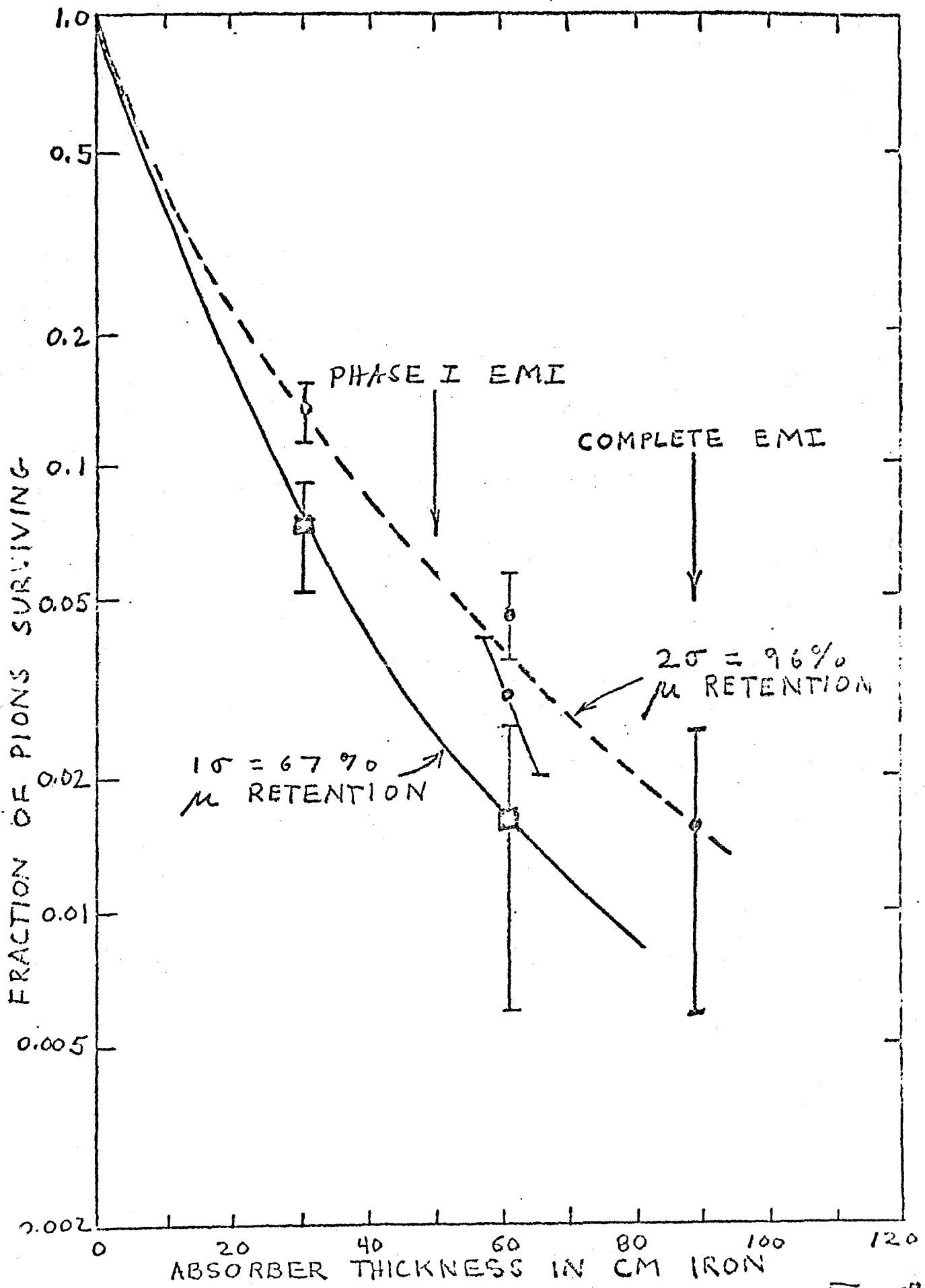


Fig. 14

9C IN NOW LISTED AS 155